

Development of Defect Verification System of IC Lead Frame Surface using a Ring-lighting

Yoshiharu Nakamura^{1,2} and Shuichi Enokida¹

¹*Kyushu Institute of Technology, 680-4 Kawadu, Izuka, Fukuoka, Japan*

²*Mitsui High Tech, Inc., 12-10-1 Komine, Yahatanishi, Kitakyusyu, Fukuoka, Japan*

Keywords: Machine Vision, Defect Detection, Multiple Light Source Imaging, IC Lead Frame.

Abstract: It is especially needed for the IC lead frames used in the manufacture of semiconductors, which require both high quality and miniaturization. To overcome above, automatic defect detection systems based on image processing methods were proposed. Especially, this paper focuses on methods using the surface normal direction to detect a deformation in flat parts. Since most of these methods use a fixed parameter, the risk of missing a defect in industrial parts becomes a problem. In this paper, new defect detection method is proposed for detecting various defect sizes and defect types. This method determines the appropriate block size based on the median value of luminance dispersions calculated for several block sizes and learning from a sample that detects a defect point beforehand. We used 105 samples in our experiments. Our experimental results show our proposed method selects the superior parameters and identification of the defect area selected is superior with learning in detecting defects of several sizes.

1 INTRODUCTION

1.1 Background of This Research

Recently, demand has grown for defect detection processes in machine vision applications. This is especially needed for the IC lead frames used in the manufacture of semiconductors, which require both high quality and miniaturization. In previous work, we proposed a detection method that assumes the variance in the intensity of oriented gradients in images having defective areas is larger than that found in normalcy areas (Nakamura et al., 2013). Therefore, detecting defects tends to have large variance in the local image (Aoki et al., 2013). We performed further experiments reported in this study by Aoki et al., for IC lead frames. However, we confirmed that detection was difficult, when these methods are used for verifying a deformation in flat parts. Image processing methods by using the surface normal direction information was proposed to detect a deformation in flat parts (Hirose et al., 2000; Morimoto et al., 2011; Tanaka et al., 1994). However, most of these methods use a fixed parameter, such as block size. When these methods look for various defects at whole images of

industrial parts by using the same parameter, the risk of missing a defect increases. In this paper, another detection method is proposed for detecting various defect sizes and defect types. To detect various defects in industrial parts with this method, it is necessary to change parameters according to the size, especially, but also the kind of defect.

1.2 Purpose

In this paper, we pay attention to the defect size to detect various defects for IC lead frames. It is supposed that a small defect is detected by using a defect detector of small block size, since a small defect has a high-frequency signal. On the other hand, it is supposed that a large defect is not detected by using a defect detector of small block size, since the large defect has a low-frequency signal. It is supposed that a defect detector of the large block size is necessary to detect the low-frequency signal. In this paper, we propose a method for automatically determining the appropriate block size for the size of the defect. Fig. 1 shows the flow of inspection processing of the proposed method.

The inspection processing comprises two phases. In the first phase (inspection processing #1), each

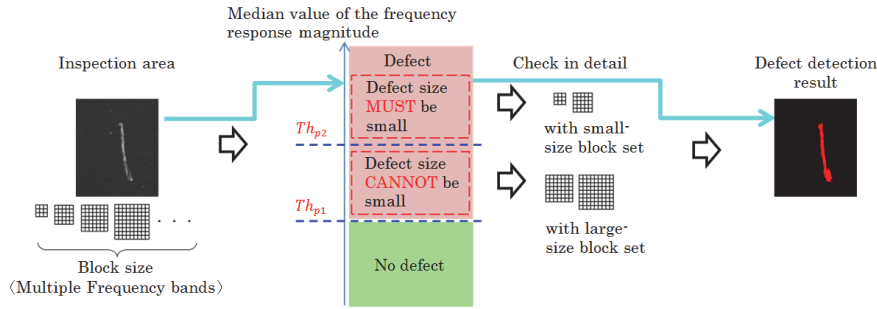


Figure 1: Flow of inspection processing of the proposed method.

inspection area is processed in all frequency bands. Inspection processing #1 has little calculation cost. A suspicious area detected in the first phase is passed to the second phase (inspection processing #2). The second phase identifies the defect position. Compared to inspection processing #1, inspection processing #2 has a high calculation cost. In the second phase, it is necessary to process a small area to identify the defect area exactly. However, processing in a small area decreases the acquired information about the defect. We complement the information so that the defect can be identified even in a small area by obtaining multiple images while the light source direction is rotated around the viewing direction. However, one risk is that the area contains a lot of noise when only high-frequency information is used. Another risk is that the number of undetected defects increases when only low-frequency information is used. Therefore, instead of using a fixed block size, we use the weighted sum of processed values in a plurality of block sizes. As a result, a defect area is identified by reducing the influence of the inclination of the optical system. The block size and weight are automatically determined by using the value in each frequency band provided from an input image directly in inspection processing #1 and learning from a sample that detects a defect point beforehand. In this paper, we use a defect detector, in which the disagreement area of the surface normal direction and the camera optical axis is defined as a defect, since the normal direction of the defect area has an inclination in comparison with that of the normalcy area. (The normalcy area is flat in an IC lead frame.)

2 RELATION OF SURFACE NORMAL DIRECTION AND REFLECTED LIGHT

2.1 Reflection Models and Relation to Surface Normal Direction

The state of light reflected from an object surface has been represented in a variety of reflection models. In many such reflection models, light values are approximated by the sum of the specular and diffuse reflection components (Mukaigawa, 2010).

Lambert models are used as a diffusion reflection model at viewpoint x of the object surface. In Eq. (1), it is assumed that the Lambert model is proportional to the cosine of the angle defined by the normal direction \mathbf{N} and the direction of light source \mathbf{L} .

$$i = \rho_d \max(0, \mathbf{N} \cdot \mathbf{L}) \quad (1)$$

where ρ_d is diffuse reflectance.

Additionally, in Eq. (2), the Phong model (Phong, 1975), which is a specular reflection model, is approximated as the power of the cosine of angle α defined by viewing direction \mathbf{V} and specular reflection \mathbf{L}' .

$$i = \rho_s \cos^n \alpha \quad (2)$$

where ρ_s is specular reflectance and n is a parameter representing the surface roughness.

The intensity of reflected light depends on the surface normal direction relative to both the diffuse reflection component (represented by the Lambert model) and the specular reflection component (represented by the Phong model). If the viewing direction is parallel to the surface normal direction, the reflected light intensity does not change when the light source direction rotates around the viewing direction. However, when the viewing direction is not parallel to the surface normal direction, the reflected light intensity

varies as the light source rotates around the viewing direction. Therefore, by obtaining and analyzing multiple images while the light source direction is rotated around the viewing direction, it is possible to determine whether the viewing direction is parallel to the surface normal direction.

2.2 Surface Normal in the Defect Area

In previous work, we proposed a detection method that assumed the variance in the intensity of oriented gradients in images that include defect areas to be larger than normalcy areas. This method targets the example defects shown in Fig. 2 and Fig. 3. In Fig. 2, the method effectively detects a defect in the end face and a defect having a strong edge. However, it could not satisfactorily detect a defect not having a strong edge and a defect shaped as a rectilinear figure in a flat area, as shown in Fig. 3. Therefore, for the defect shown in Fig. 3, we use a defect detector in which the disagreement area of the surface normal direction and the camera optical axis is defined as a defect, since more inclination is found in the surface normal direction than in the normalcy area in the defect area due to the normalcy area being flat in IC lead frames. The inclinations of the surface normal directions in the defect area are shown in Fig. 3.

as the light source rotates around the viewing direction.

Therefore, by obtaining and analyzing multiple images while the light source direction is rotated around the viewing direction, we are able to determine whether a defect is detected. Originally, it was expected that detection of a defect was possible, when the shape of the defect was estimated by using the photometric stereo method (Woodham, 1980) with multiple light sources. However, the estimate of a detailed shape had a high calculation cost. In addition, since the information that we want to get is whether a defect exists, detailed shape information is not required. Therefore, we decided to apply the proposed method, which identifies only the reflection intensity of light changes by the inclination of the normal direction.

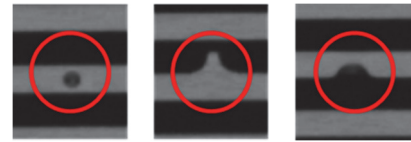


Figure 2: Defect with variance in the intensity of oriented gradients.

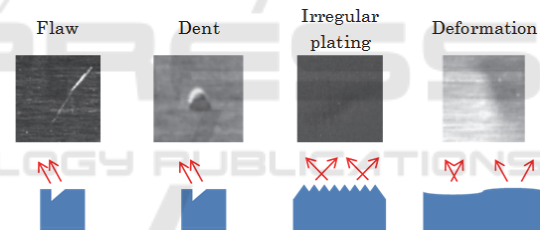


Figure 3: Defects and surface normal directions.

3 INSPECTION METHOD

3.1 Inspection Equipment

Fig. 4 shows the experimental environment used to acquire images. We rotated a light emitting diode (LED) ring-lighting, which opening 90° in 22.5° increments in order to acquire 16 images while varying the direction of incident illumination.

3.2 Agreement or Disagreement of Normal Direction and Camera Optical Axis

In this paper, defects are detected by using the variance calculated by using multiple images acquired by varying the light source direction. If the viewing direction is parallel to the surface normal direction, the reflected light intensity does not change when the light source direction rotates around the viewing direction. However, when the viewing direction is not parallel to the surface normal direction, the reflected light intensity varies

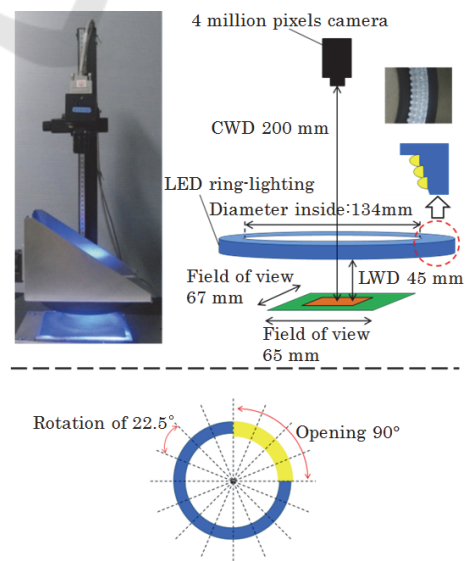


Figure 4: Imaging environment.

3.3 Inspection Processing

As mentioned above, the inspection processing comprises two phases. The first phase determines whether a defect exists for each inspection area (inspection processing #1). The second phase identifies a defect area for an area determined to include a defect in inspection processing #1 (inspection processing #2).

3.3.1 Inspection Processing #1: Determining Whether a Defect Exists

The first phase determines whether a defect exists for each inspection area. The variance value V_r is used for the determination. V_r determines a defect by identifying the areas of brightness change by the inclination of the normal direction of the defect in a large area. V_r can determine a defect if a defect having a different brightness is in the peripheral area, because the variance values of the block are increased. V_r is calculated by using the maximum of the measured variance values. These values are calculated for N ($i=1, 2 \dots N$) images acquired from several light source directions (Fig. 5). By using the maximum value, it is possible to use a light source direction in which the defect has the largest brightness difference.

$$V_r^{(i)}(x, y) = \frac{1}{s_r^2} \sum_{x=1}^{s_r} \sum_{y=1}^{s_r} (I_{x,y} - \bar{I}_r)^2 \quad (3)$$

$$V_r(x, y) = \max_{i \in N} \{V_r^{(i)}(x, y)\}$$

where s_r is block size, \bar{I}_r is the mean in the block.

A raster scan of the inspection area is performed and V_r is computed for all pixels using Eq. (3).

To detect defects having various frequency bands, various block sizes are prepared. The processing calculates the maximum value of V_r for each different block size, and then obtains the median value from the maximum value for each different block size (median V_r). The proposed method compares median V_r with the threshold Th_{p1} .

$$\begin{aligned} \text{median}V_r &= \text{median}_{s_r} [\max_x \{V_r(x, s_r)\}] \\ \text{median}V_r &> Th_{p1} \end{aligned} \quad (4)$$

where x is the position the inspection area.

By using the median value from the maximum value for each different block size, if a defect exists, the V_r value is larger for that block size. Then, the existence of a defect can be determined robustly, while reducing the influence of noise in a particular block size.

3.3.2 Inspection Processing #2: Defect Area Is Identified

In the second phase, a defect area is identified for an area already determined to include a defect in inspection processing #1. It is necessary to process a small area to identify a defect area exactly. If the block size is small, V_r values used in inspection processing #1 cannot obtain sufficient variance values for the defect, since V_r values are calculated for each light source direction. Therefore, V_d is used to determine whether the normal direction at the point (or small region) of interest is parallel to the camera's optical axis. V_d is calculated in the same block by using multiple images, which are acquired by varying the N ($i = 1, 2 \dots N$) direction of the light source (Fig. 6).

$$V_d(x, y) = \frac{1}{N \cdot s_d^2} \sum_{i=1}^N \sum_{x=1}^{s_d} \sum_{y=1}^{s_d} (I_{i,x,y} - \bar{I}_d)^2 \quad (5)$$

where s_d is block size, \bar{I}_d is the mean in the block.

A raster scan of the inspection area is performed and V_d is then computed for all pixels by Eq. (5). This value of V_d is used to determine whether the normal direction at the point (or small region) of interest is parallel to the camera's optical axis. However, this assessment alone is inadequate when the stage has only a slight tilt with respect to the optical axis (Fig. 7) and has a lot of noise. Therefore, V_r must overcome this problem. Because V_r is capable of discriminating between the flat and curved areas at a (large) surface area of interest, it overcomes the problem that results when the stage is tilted with respect to the optical axis. Finally, the weighted sum of V_d and V_r is utilized to detect defects. V_d and V_r are normalized at each maximum. Defect detection is then performed by using α , which determines the weight of the V_d value, the V_r value, and Th , which determines the detection level.

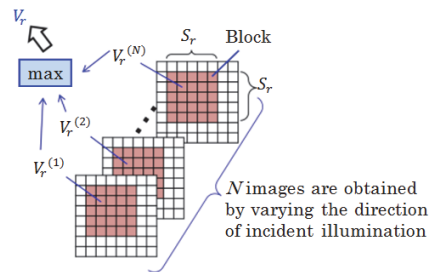
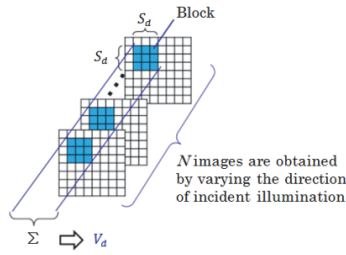


Figure 5: V_r calculation method.


 Figure 6: V_d calculation method.

$$(1 - \alpha) \frac{V_d(x, y)}{\max V_d} + \alpha \frac{V_r(x, y)}{\max V_r} > Th \quad (6)$$

The block sizes used for V_d and V_r that make $s_r > s_d$ because V_d is calculated in a small region and V_r is calculated in a large region.

In the inspection, the determination of each parameter (block size set (s_d, s_r) , α , Th) is important. Each parameter is automatically determined by learning with some samples containing a defect. The f -measure, which is the harmonic average of the ratio of the detected area to the total correct answer area and ratio of the correct answer area to the total detected area, is used as a learning indicator. (By using the harmonic average, if the one is remarkably lower than the other, the influence of the one is suppressed.) The determination of the block size set uses the median V_r value calculated for each inspection area in inspection processing #1. If the median V_r value is large, because it is presumed that a high-frequency defect exists, it is necessary to find the exact defect area by using a small block size set. If median V_r value is small, because it is presumed that a low-frequency defect exists, it is necessary to find the defect in a large area by using a large block size set. The flow of learning is shown below (Fig. 8).

- (i) First, in order to determine α and Th for each block size set, the defect area is detected and the f -measure is calculated by Eq. (6) and using the learning defect samples. The average of the f -measure of all defect samples is calculated (\hat{f} -measure), and α and Th are determined by the biggest \hat{f} -measure for each block size set.
- (ii) The block size set is determined for each defect sample. Th_{p2} is assigned to separate each defect sample so that the f -measure is bigger. Fig. 8 (ii) are plots with the median V_r of each defect sample and the f -measure with α and Th determined in (i). The block size set is determined by whether median V_r of each defect sample is larger or smaller than Th_{p2} .

- (iii) The average of the f -measure (\hat{f} -measure) is calculated at each block size set determined for each defect sample, and the final α and Th are determined by the biggest \hat{f} -measure for each block size set.

It is necessary to repeat (ii) and (iii) to obtain the necessary precision. An area is inspected by using each determined parameter.

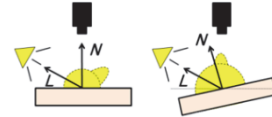


Figure 7: Proper and improper optical system alignments. Left: Ideal condition, Right: Lead frame inclining in relation to the camera.

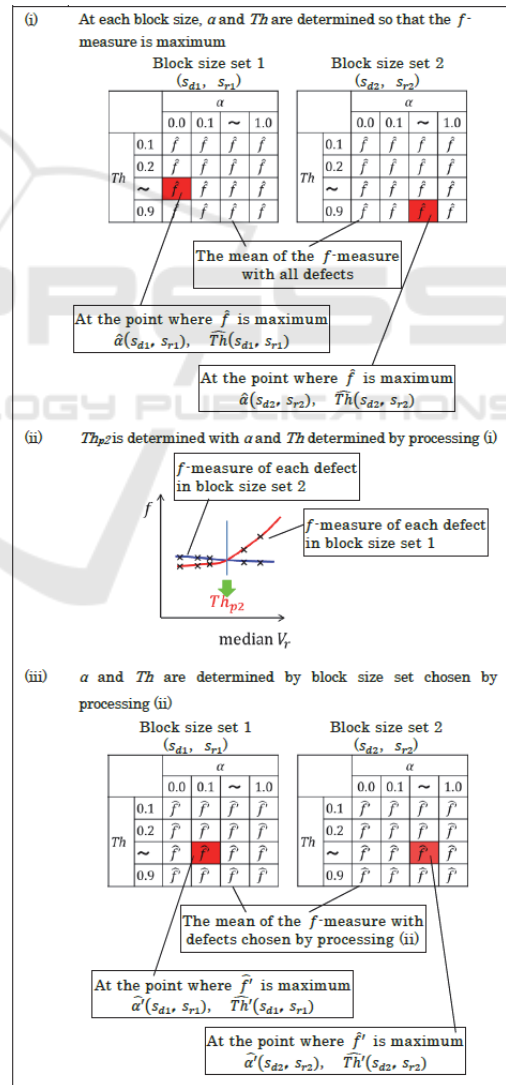


Figure 8: Self-adjusting parameters.

4 EXPERIMENTS AND RESULTS

4.1 Test Sample and Images

We used 105 samples in our experiments (Defect-free samples: 41, Flaw: 16, Dent: 16, Irregular plating: 16, Deformation: 16). Fig. 9 shows an example of an IC lead frame that has a flaw in the center. Multiple images of each defect were acquired from the 16 light source directions (Fig. 10). In our experiment, each sample was processed by inspection processing #1 and inspection processing #2.

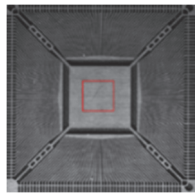


Figure 9: IC lead frame with a flaw.

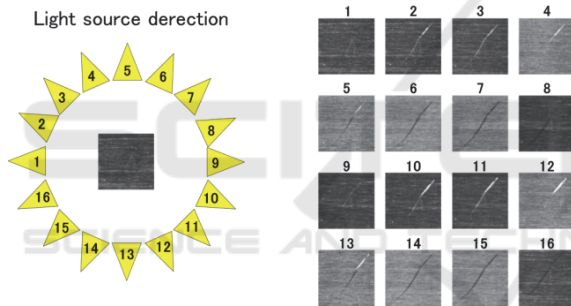


Figure 10: Multiple light source imaging.

4.2 Results of Determination of the Parameters by the Learning

The results of defect detection based on the parameters of block sizes s_d and s_r , weight α , and threshold Th , which are automatically determined by learning, are shown in Figs. 11–13. In this experiment, because it was a fundamental experiment to identify the performance of the proposed method, a block size set was either a large set or a small set ($(s_d, s_r) = (3, 9)$ or $(s_d, s_r) = (5, 25)$), and the learning was 1 loop (s_d and s_r were appropriately examined in the experiment). The results of these three figures are shown from top to bottom in the following order: original image—correct answer image—result of the parameter when the \hat{f} -measure is the largest in the small block size set without learning—result of the parameter when

the \hat{f} -measure is the largest in the large block size set without learning—result of the parameter that is automatically determined by the proposed method.

Fig. 11 shows examples of the results determined to be in the small block size set by the proposed method. Fig. 12 shows examples of the results determined to be in the large block size set by the proposed method. By comparing the results of the proposed method with the results of each block size set without learning, it was confirmed in Figs. 11 and 12 that identification of the defect area selected was superior with learning. This result shows that the method selected the superior block size set and α and Th were changed to more appropriate values. However, in some cases the method failed to select the superior block size set. Examples that failed in the selection of the block size sets are shown in Fig. 13. These were selected to be in the block size set “large” by the proposed method. However, the block size set “small” was accurate for identification of the defect area, according to the images without learning. It is possible that learning became specialized for a learning sample. Therefore, it is necessary to examine a learning method not specialized for a defect sample as a future problem.

4.3 Results of Inspection Processing #1

4.3.1 Experimental Condition

For all 105 samples, inspection process #1 determined whether a defect existed for each inspection area. The variance for detecting a defect at each inspection area was V_r . The following block sizes were examined in the experiment: $s_r = 9, 17, 25, 33, 41, \text{ and } 49$. Median V_r was calculated for each defect sample. Then, median V_r was compared to the threshold to determine whether it was a defect. A brightness difference occurs with each image acquired by varying the light source direction, as shown in Fig. 14 for processing a hairline on a surface. It was confirmed that the separation of the defect was difficult in a prior experiment. Therefore, we used only a parallel light source direction for the hairline (light source directions are #1, 2, 8, 9, 10, and 16 in Fig. 10).

4.3.2 Results of Experiment and Discussion

In the defect inspection experiment, we analyzed a characteristic of the proposed method with two thresholds. The first is the threshold when the recall ratio of the defect is 100% and false positives (false detection) are minimum.

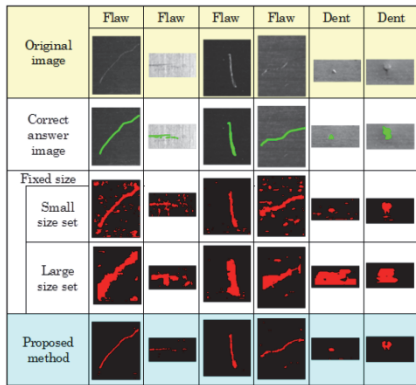


Figure 11: Examples of “the block size set is small”.

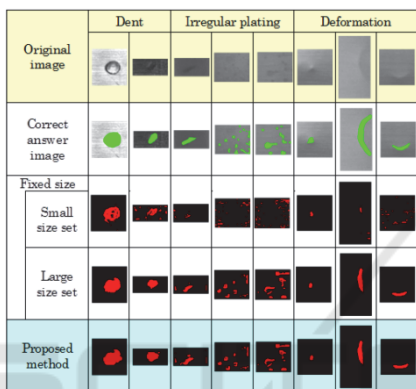


Figure 12: Examples of “the block size set is large”.

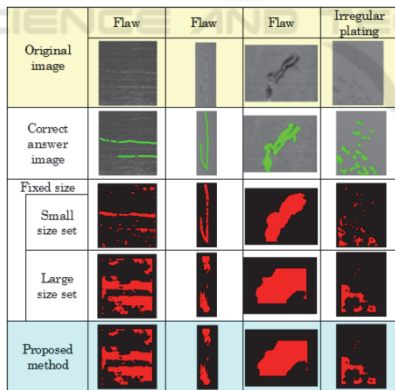


Figure 13: Examples of failed selection.

The second is the threshold when the precision ratio is 100% and false negatives (overlooking) are minimum. With the first threshold, 6 samples were detected as a defect among 41 defect-free samples. The examples of false detection are shown in Fig. 15. According to Fig. 15, defects were detected excessively for the sensitive threshold, since multiple points with brightness differences exist. It is thought that these should be reexamined rather

than overlooked, since these are difficult to classify as a defect of a flaw or irregular plating. With the second threshold, 3 samples were overlooked as a defect among 64 defect samples. The examples of overlooked samples are shown in Fig. 16. According to Fig. 16, the defect of a small brightness difference was overlooked. In inspection processing #1, it is thought that the excessive threshold should be used, because it is necessary to prevent overlooking defects, even if some defect-free products are detected as defects. Therefore, the first threshold should be used. The results show that the proposed method is effective for the detection of defects of various types and sizes.

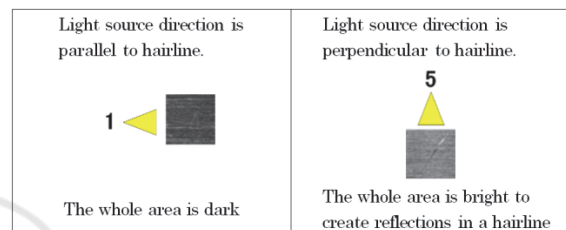


Figure 14: Hairline on surface and light source direction.

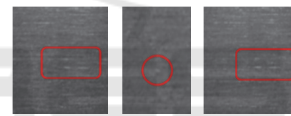


Figure 15: Examples of error detection images.

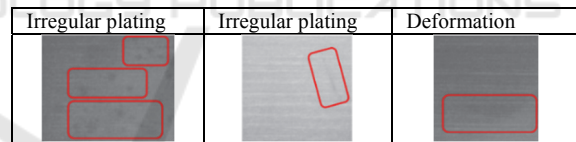


Figure 16: Examples of undetected images.

4.4 Results of Inspection Processing #2

4.4.1 Experimental Condition

In this experiment, defect areas are identified for 64 defect samples. These 64 samples are distributed into 4 sets of 16 samples, and 3 sets are used for learning to determine the parameter, and we evaluate the detection with the one remaining set. The data set is replaced and new learning and data sets are created, then assessed 4 times. As mentioned in Section 3, a brightness difference occurs with each image acquired by varying the light source direction, since the processing was for a hairlined surface. Therefore, we used each image by flattening the histogram.

4.4.2 Results of Experiment and Discussion

As the results of 4 iterations of evaluation by replacing the data set, the rate of success of identifying a defect area was 84.4%. Examples of successful specific defect areas are shown in Fig. 17. Examples of failure detections are shown in Fig. 18.

In this experiment, when identification of a defect area was investigated for each kind of defect, it was confirmed that a deformation could be identified in all samples. The proposed method identified all cases of a deformation with a large normal change, by judging whether the camera optical axis was parallel to the normal direction.

However, identification failed in the case of some of the other types of defects.

For the dent and the irregular plating, a tendency of failure of common defect identification was confirmed. A large area other than the defect area was detected. The dent had a rapid change in the normal direction, however, the defect area was too small. Irregular plating had too small a brightness as compared with the peripheral area. Therefore, separation of the intensity variation of the background texture was difficult when such defect areas were identified. To further improve the performance, a way to establish a parameter apart from a parameter of deformation with a large normal change must be considered. We will investigate the parameters of the method in the future.

For the flaw, both of the areas were detected excessively and areas with a defect were overlooked. In the proposed method, we conclude that it is difficult to classify a surface hairline, such as a linear defect (flaw). For detecting a defect such as a flaw, we consider it necessary to improve the precision in combination with image processing techniques shown in previous work (Nakamura et al., 2013).

	Flaw	Dent	Irregular plating	Deformation
Original image				
Correct answer image				
Defect detection Result				

Figure 17: Examples of successful detection images.

	Dent	Irregular plating	Flaw
Original image			
Correct answer image			
Defect detection Result			

Figure 18: Examples of error detection images.

5 CONCLUSIONS

In this paper, we propose a method for automatically determining the appropriate block size for the size of defects to detect defects of various sizes that occur in the surface of IC lead frames. We showed that it was possible to detect defects that were previously difficult to identify by conventional methods. We used the weighted sum of two values. The one is that identify the areas of changing brightness by the inclination of the normal direction of the defect in a large area. The other is that determines whether the normal direction at a point of interest is parallel to the camera’s optical axis by using the inclination of the normal direction on the surface of the defect area. As future work, it is necessary to examine a learning method that is not specialized for a defect sample. We are also planning to develop a system that can detect whole parts by using the image processing method that detects the end face of a part together with the proposed method that detects the flat area of a part.

REFERENCES

- Nakamura, Y., Masuzoe, M., & Enokida, S., 2013. Study of Defect Verification based on Histogram of Oriented Gradients in Local Area. *The Institute of Image Electronics Engineers of Japan, 264th study meeting.*
- Aoki, K., Funahashi, T., Koshimizu, H., & Miwata, Y., 2013. “KIZUKI” Algorithm Inspired by Peripheral Vision and Involuntary Eye Movement. *Journal of the Japan Society for Precision Engineering*, Vol. 79, No. 11, 1045-1049.
- Hirose, O., Ishii, A., Hata, S., & Washizaki, I., 2000. Detection of Small Convex and Concave Defects on Optical Films by Patterned Illumination. *Journal of the Japan Society of Precision Engineering*, Vol. 66, No. 7, 1098-1102.
- Morimoto, Y., Fujigaki, M., & Masaya, A., 2011.

- Displacement and Strain Distribution Measurement by Sampling Moire Method. *Journal of the Vacuum Society of Japan*, Vol. 54, No. 1, 32-38.
- Tanaka, K., Shinbara, Y., Ikeda, H., Yamada N., Kiba, H., & Sasanishi. K., 1994. Automated Inspection Method for Painted Surfaces. *Transactions of the Japan Society of Mechanical Engineers, C* 60(577), 3201-3208.
- Mukaigawa, Y., 2010. Measurement and Modeling of Reflection and Scattering. *IP SJ SIG Technical Report*, Vol. 2010-CVIM-172, No. 34.
- Phong. B. T., 1975. Illumination for Computer Generated Pictures. *Proc. SIGGRAPH'75*, 311-317.
- Woodham, R. J., 1980. Photometric Method for Determining Sur-Face Orientations from Multiple Images. *Optical Eng.*, 19, 139-144.

